International Journal of Mechanical and Electrical Engineering
ISSN: 3005-9615 (Print), ISSN: 3005-7132 (Online)
Volume 8, Number 6, Year 2026
DOI: https://doi.org/10.62051/ijmee.v8n6.06

Experimental Strain Correction of a Cantilever Beam Using DQEM Computational Labels and Weak Mechanics-Informed Regularization

Yuan Shu

University of Shanghai for Science and Technology, Shanghai, China

ABSTRACT

Systematic discrepancies between experimentally measured and numerically predicted strains can limit model validation and subsequent data-driven analysis. This study develops an experimental strain correction framework for a multi-point loaded cantilever beam using differential quadrature element method (DQEM) computational labels, ANSYS finite element validation, and weak mechanics-informed regularization. A total of 258 loading cases were analyzed at five strain-measurement locations. The DQEM labels showed good agreement with ANSYS, with a full-sample MAE of 1.6694 με. A point-wise correction model was then trained using experimental variables and a weak Euler–Bernoulli bending regularization term. On a load-case-level test set, the proposed model achieved an MAE of 1.8447 με and an RMSE of 5.8143 με. Compared with the uncorrected experimental data, the corrected results substantially reduced strain error while maintaining stable performance under noise perturbation. The results demonstrate that validated computational labels combined with weak mechanics-informed learning provide a practical approach for correcting systematic strain-measurement errors.

KEYWORDS

Cantilever Beam; Differential Quadrature Element Method; Finite Element Validation; Strain Correction; Mechanics-informed Regularization.

1. INTRODUCTION

Cantilever beams are common benchmark structures in structural monitoring, load identification, and model validation because their boundary conditions are clear and their strain response is sensitive to loading [4][5]. In experiments, however, measured strain may deviate systematically from numerical predictions because of sensor placement errors, clamping uncertainty, calibration bias, and other test imperfections. Such discrepancies can reduce the reliability of numerical–experimental comparisons and data-driven models.

Existing studies have addressed strain-based load identification, structural response reconstruction, finite element model updating, and physics-informed machine learning [6][7][8]. These methods demonstrate the value of combining measured data with mechanical knowledge, but fewer studies focus specifically on correcting systematic experimental strain errors using independently validated computational labels under multiple loading cases [11][12]. This motivates a correction strategy that preserves data adaptability while introducing only a weak mechanical constraint [13][14].

Accordingly, this study follows three steps: DQEM is used to compute nonlinear static strain responses for 258 loading cases; the computational labels are independently checked against ANSYS;

Content from this work may be used under the terms of CC BY-NC 4.0 licence (https://creativecommons.org/licenses/by-nc/4.0/).
Published by Warwick Evans Publishing.

and a point-wise correction model with weak Euler–Bernoulli regularization is trained to map measured strains toward the validated computational response.

The main contribution is a compact numerical–experimental correction framework that combines DQEM–ANSYS consistency validation, full-sample error assessment, and mechanics-informed strain correction under a common load-case-level evaluation scheme.

2. TEST SPECIMEN AND EXPERIMENTAL SYSTEM

The specimen is a rectangular steel cantilever beam with length L = 1.0 m, width b = 0.08 m, thickness h = 0.01 m, Young's modulus E = 2.06 × 10^11 Pa, Poisson's ratio ν = 0.30, and density ρ = 7850 kg/m³. Four loading positions are located along the beam, and five strain gauges are arranged on the upper surface to capture the longitudinal bending strain.

The experimental system includes a clamping fixture, dead-weight loading device, strain gauges, and an NI cDAQ-9178/NI 9236 acquisition system. For each load case, the weights are applied after the beam is fully clamped, and the stabilized strain values are recorded. The dataset contains 258 experimentally feasible loading cases. To prevent leakage among measurement points from the same case, all model training and testing are split at the load-case level rather than at the individual sample level.

Table 1. Composition of Load Cases and Dataset Split

Loading type	Criterion	Number of load cases	Number of measurement-point samples
Single-point loading	1 nonzero loading point	20	100
Two-point loading	2 nonzero loading points	150	750
Three-point loading	3 nonzero loading points	61	305
Four-point loading	4 nonzero loading points	27	135
Total	258 cases; 5 measurement points per case	258	1290

The 258 cases were selected according to experimental operability, load-range coverage, and equipment safety; they do not represent all possible combinations of the four loading points.

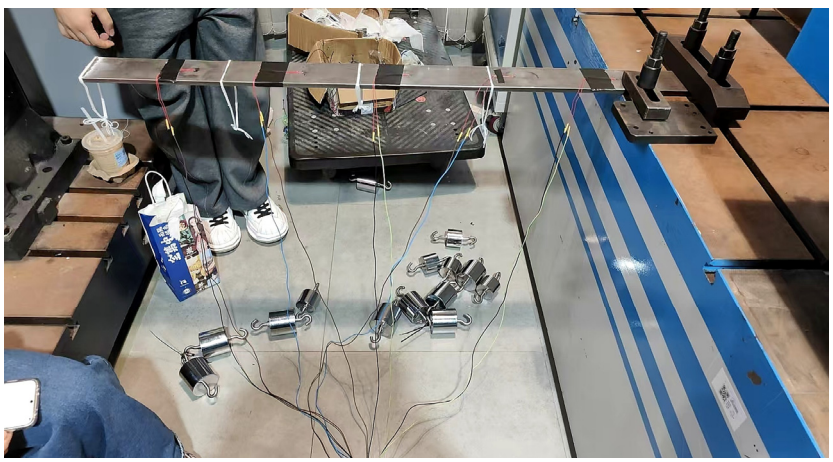


Figure 1. Overall View of the Experimental Setup

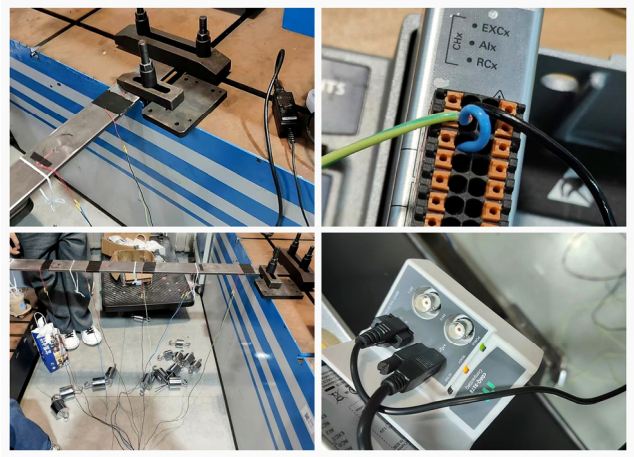


Figure 2. Key Components of the Experimental System

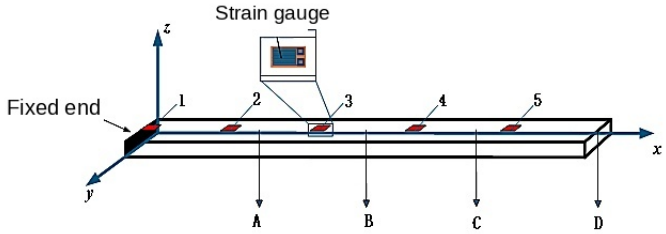


Figure 3. Schematic of the Beam, Loading Points, and Measurement Locations

3. METHODOLOGY

The method includes nonlinear static DQEM analysis, ANSYS finite element comparison, and point-wise experimental strain correction with weak mechanics-informed regularization.

3.1 Nonlinear Static Equilibrium Solution

For each loading case, the geometrically nonlinear static response is solved using DQEM discrete equilibrium equations and Newton iteration [1][3]. The nonlinear residual is written in the standard form R(q) = 0, where q denotes the generalized displacement vector. At each load step, the tangent system is solved iteratively until the prescribed residual tolerance is satisfied.

$$R(\mathbf{u}) = \mathbf{f}_{\text{int}}(\mathbf{u}) - \mathbf{f}_{\text{ext}} = \mathbf{0} \tag{1}$$

$$\mathbf{K}_t(\mathbf{u}^k)\Delta\mathbf{u}^k = -\mathbf{R}(\mathbf{u}^k), \quad \mathbf{u}^{k+1} = \mathbf{u}^k + \Delta\mathbf{u}^k \tag{2}$$

The beam is divided into four DQEM elements, each using 11 Chebyshev-distributed collocation points [2]. Shared element boundaries are merged to maintain continuity. The same geometry, material parameters, loading positions, and strain-measurement coordinates are used throughout the numerical comparison.

Loading is applied incrementally in 50 substeps. Newton iteration uses an infinity-norm residual tolerance of 1.0 × 10^-4 with a maximum of 50 iterations per substep. Non-converged cases are excluded from label generation.

3.2 Strain Extraction at Measurement Locations

The upper-surface axial strain is obtained from the beam curvature as ε_DQEM = −(h/2)κ, where κ is calculated from the nonlinear displacement/rotation field. Strains are extracted at the calibrated experimental measurement coordinates.

$$\varepsilon_{\mathrm{DQEM}} = -\frac{h}{2}\kappa \tag{3}$$

Because the strain gradient is highest near the clamped end, coordinate consistency between numerical extraction points and physical gauges is particularly important for reducing artificial comparison errors.

3.3 Mechanics-Informed Error Correction

The correction model uses a long-format dataset in which each row represents one measurement location from one loading case. Inputs include the experimental strain and loading/location information, while the DQEM strain serves as the computational target. All points from the same loading case remain in the same training or test subset.

$$L_{\mathrm{data}} = \frac{1}{N}\sum_{i}(\delta_i - \delta_i^*)^2, \quad \delta_i^* = \varepsilon_{\mathrm{DQEM},i} - \varepsilon_{\mathrm{exp},i} \tag{4}$$

$$L_{\mathrm{phy}} = \frac{1}{N}\sum_{i}\left(\delta_i - \delta_{\mathrm{EB},i}\right)^2 \tag{5}$$

$$L = L_{\mathrm{data}} + \lambda L_{\mathrm{phy}} + \beta \parallel \theta \parallel_2^2 \tag{6}$$

A weak Euler–Bernoulli bending term is added to the data loss as mechanics-informed regularization [9]. For each sample, the approximate bending moment is calculated from the applied loads and measurement position, and the corresponding beam-theory strain provides a soft physical reference. The total loss combines prediction error and the weighted physics term, allowing the model to follow the data while discouraging mechanically implausible predictions.

The regularization coefficient was selected from $\lambda \in \{0, 0.05, 0.10, 0.20, 0.50\}$. With random seed 42 and 3000 training epochs, $\lambda = 0.20$ was used for the main model based on the combined test accuracy and robustness results.

The regularization is intentionally weak: it does not force the prediction to satisfy an ideal beam equation exactly, but introduces a mechanical trend that improves stability when experimental data contain noise or when unseen load cases are evaluated.

4. CONSISTENCY VALIDATION AND COMPARATIVE ANALYSIS

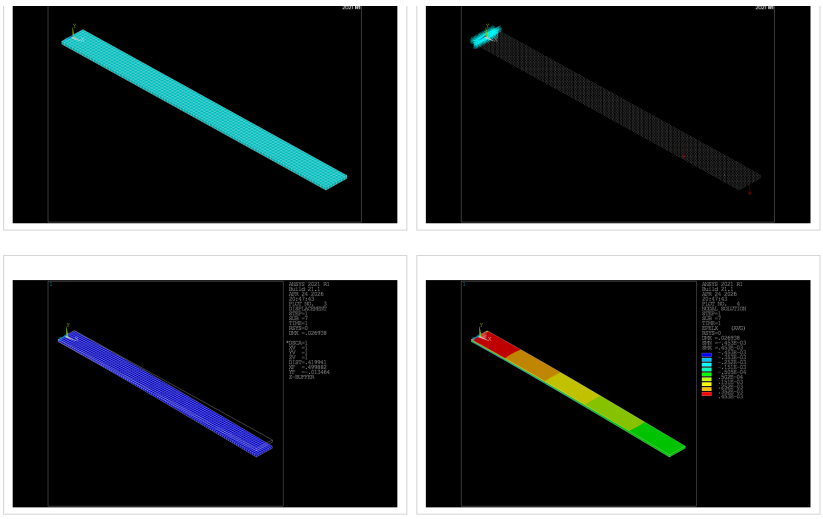


Figure 4. ANSYS Finite Element Model and Response Results: (a) Geometry and Mesh; (b) Fixed Constraint and Loads; (c) Displacement Contour; (d) EPEL,X Strain Contour

The DQEM labels are compared with an ANSYS finite element model using the same beam geometry, material parameters, boundary condition, and loads [10]. The ANSYS model employs SOLID186 elements [15]. Longitudinal elastic strain at the five measurement locations is extracted for all 258 load cases and compared with the corresponding DQEM values.

Because the through-thickness mesh is limited, ANSYS is used as an independent consistency reference rather than as an exact local-stress benchmark. The comparison therefore focuses on overall agreement across the complete dataset.

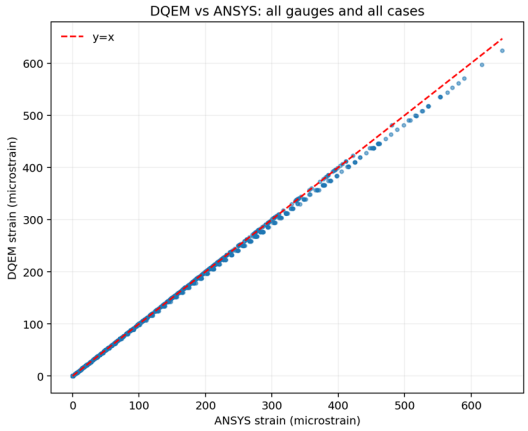


Figure 5. Full-Sample Comparison Between DQEM and Finite Element Results

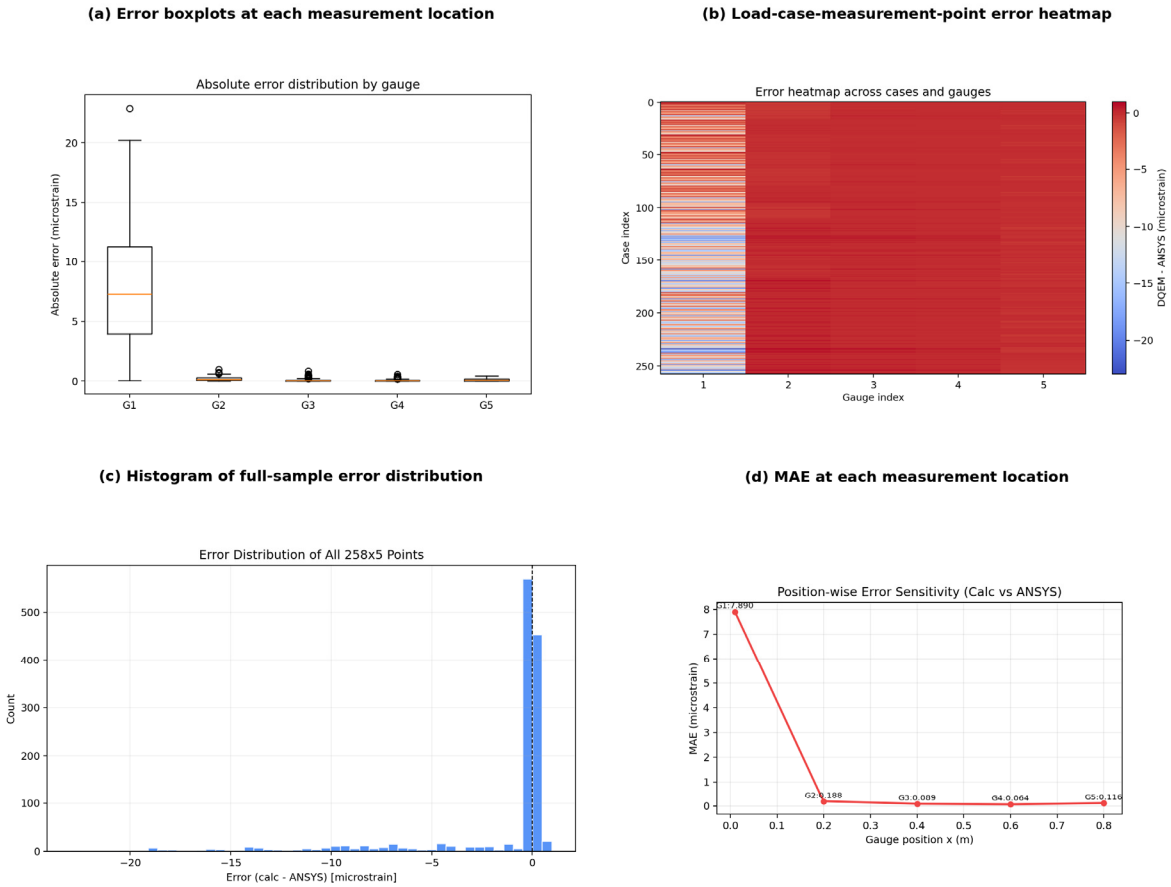


Figure 6. Error Statistics for the DQEM–ANSYS Comparison: (a) Error Boxplots at Each Measurement Location; (b) Load-Case–Measurement-Point Error Heatmap; (c) Histogram of Full-Sample Error Distribution; (d) MAE at Each Measurement Location

Across 258 load cases and 1,290 measurement-point samples, DQEM and ANSYS show good consistency, with an MAE of 1.6694 με. Larger local errors mainly occur in high-strain regions near the clamped end, whereas the overall error distribution remains concentrated at low values. These results support the use of the DQEM output as computational labels for subsequent experimental strain correction.

5. EVALUATION AND DISCUSSION OF CORRECTION PERFORMANCE

Using the same load-case-level split, the proposed model is compared with linear regression, quadratic regression, a regression tree, and a bagged ensemble. Performance is evaluated using MAE and RMSE, together with the reduction in error relative to the raw experimental strains.

Table 2. Error Comparison of Different Models on the Load-Case-Level Test Set

Model	MAE (με)	RMSE (με)	MAPE (|ε| ≥ 10 με, %)
Uncorrected experimental strain	22.1758	30.9444	15.8584
Linear	3.6080	7.7357	4.2103
Poly2	3.3002	7.5458	3.4974
Tree	1.8501	6.9482	2.2083
EnsembleBag	2.3869	7.4825	2.6070
Proposed model (λ = 0.20)	1.8447	5.8143	2.7770

Note: To avoid abnormally amplified relative errors when the reference strain is close to zero, MAPE is calculated only for samples with |ε| ≥ 10 με.

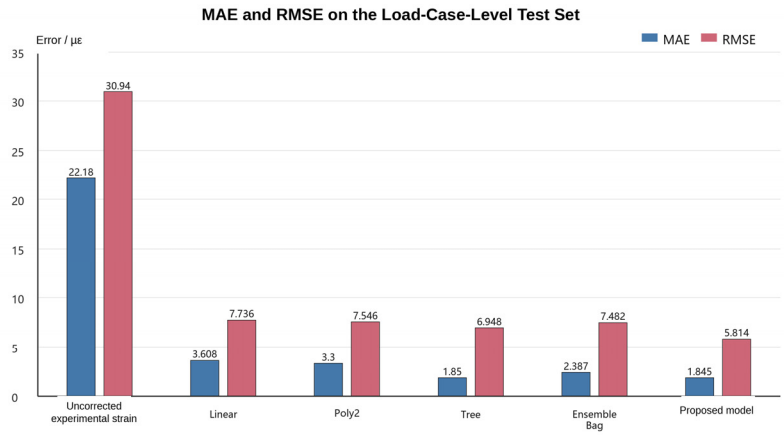


Figure 7. Comparison of MAE and RMSE for Different Models on the Load-Case-Level Test Set

With λ = 0.20, the proposed model achieves an MAE of 1.8447 με and an RMSE of 5.8143 με. The regression-tree baseline gives an MAE of 1.8501 με, indicating only a small difference in nominal test accuracy. The main value of the mechanics-informed term is therefore not a large reduction in average error over the strongest baseline, but improved physical regularization and stable behavior under perturbation, as supported by the ablation and noise tests in Fig. 8.

The correction effect is more evident relative to the raw measurements. Against the DQEM labels, the uncorrected experimental strains produce an MAE of 22.1758 με, whereas the corrected predictions reduce the MAE to 1.8447 με. This shows that the model mainly serves to remove

systematic experimental–numerical discrepancies rather than to outperform conventional regressors by a large margin.

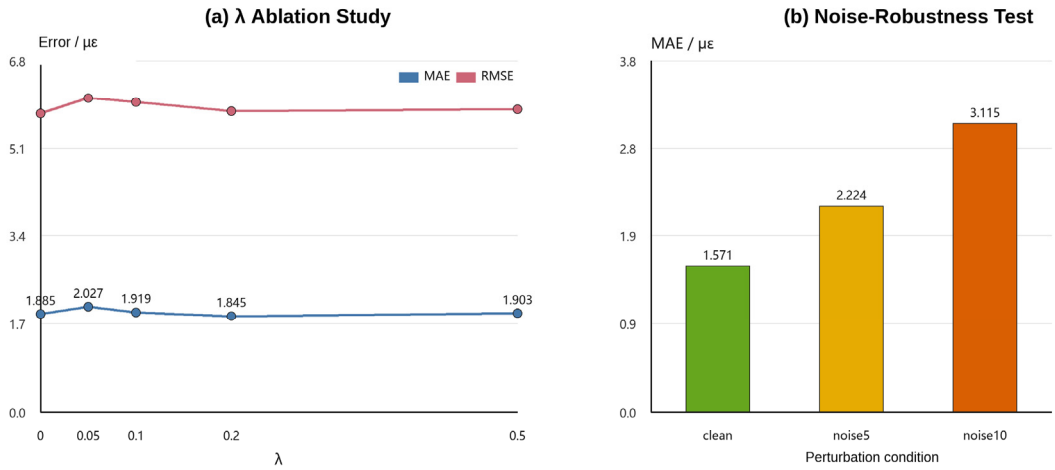


Figure 8. Ablation and Noise-Robustness Tests: (a) λ Ablation Study; (b) Noise-Robustness Test

5.1 Limitations

This study has several limitations. The experiments are limited to static loading, repeated-test uncertainty was not fully quantified, and the finite element model was used primarily for consistency validation rather than detailed mesh-convergence analysis. In addition, the gain over the strongest purely data-driven baseline is modest, so broader datasets are needed to assess generalization.

6. CONCLUSION

A strain correction framework combining DQEM computational labels, ANSYS consistency validation, and weak mechanics-informed regularization was developed for a multi-point loaded cantilever beam. The DQEM results agreed well with ANSYS over 1,290 samples, supporting their use as computational labels. The proposed correction model reduced the experimental strain MAE from 22.1758 με to 1.8447 με on the load-case-level test set. Although its nominal MAE is close to that of the best conventional baseline, the weak mechanical regularization provides an explicit physical trend and improves robustness without imposing a strict governing-equation constraint.

Future work will extend the method to dynamic loading, repeated-test validation, mesh-sensitivity studies, and transfer across specimens and operating conditions.

REFERENCES

[1] Bellman, R., & Casti, J. (1971). Differential quadrature and long-term integration. Journal of Mathematical Analysis and Applications, 34(2), 235–238. https://doi.org/10.1016/0022-247X(71)90064-5.

[2] Shu, C. (2000). Differential quadrature and its application in engineering. Springer. https://doi.org/10.1007/978-1-4471-0379-8.

[3] Bert, C. W., Wang, X., & Striz, A. G. (1993). Differential quadrature for static and free vibration analyses of anisotropic plates. International Journal of Solids and Structures, 30(13), 1737–1744. https://doi.org/10.1016/0020-7683(93)90037-4.

[4] Hong, W. C., Wang, Y. J., Chen, C. Y., & Su, H. J. (2013). A strain-based load identification model for beams in building structures. Sensors, 13(8), 9909–9927. https://doi.org/10.3390/s130809909.

[5] Song, X. D., Wang, Y., & Zhao, Y. (2017). Load identification for a cantilever beam based on fiber Bragg grating sensors. Sensors, 17(8), 1733. https://doi.org/10.3390/s17081733.

[6] Liu, X., Liu, H., Chen, Z., He, J., & Zhou, X. (2018). Inverse finite element method for reconstruction of deformation in the gantry structure of heavy-duty machine tool using FBG sensors. Sensors, 18(7), 2173. https://doi.org/10.3390/s18072173

[7] Mottershead, J. E., & Friswell, M. I. (1993). Model updating in structural dynamics: A survey. Journal of Sound and Vibration, 167(2), 347–375. https://doi.org/10.1016/0022-460X(93)90345-B.

[8] Friswell, M. I., & Mottershead, J. E. (1995). Finite element model updating in structural dynamics. Kluwer Academic Publishers.

[9] Timoshenko, S. P., & Gere, J. M. (1972). Mechanics of materials. Van Nostrand Reinhold.

[10] Hughes, T. J. R. (1987). The finite element method: Linear static and dynamic finite element analysis. Prentice-Hall.

[11] Raissi, M., Perdikaris, P., & Karniadakis, G. E. (2019). Physics-informed neural networks: A deep learning framework for solving forward and inverse problems involving nonlinear partial differential equations. Journal of Computational Physics, 378, 686–707. https://doi.org/10.1016/j.jcp.2018.10.045.

[12] Karniadakis, G. E., Kevrekidis, I. G., Lu, L., Perdikaris, P., Wang, S., & Yang, L. (2021). Physics-informed machine learning. Nature Reviews Physics, 3(6), 422–440. https://doi.org/10.1038/s42254-021-00314-5.

[13] Willard, J., Jia, X., Xu, S., Steinbach, M., & Kumar, V. (2022). Integrating scientific knowledge with machine learning for engineering and environmental systems. ACM Computing Surveys, 55(4), 1–37. https://doi.org/10.1145/3491278

[14] Al-Adly, A., & Kripakaran, P. (2024). Physics-informed neural networks for structural health monitoring: A case study for Kirchhoff-Love plates. Data-Centric Engineering, 5, e6. https://doi.org/10.1017/dce.2024.3.

[15] ANSYS Inc. (2024). Mechanical APDL theory reference. ANSYS Inc.